

1 Aggregation of nontuberculous mycobacteria is regulated by carbon:nitrogen balance

2

3 William H. DePas¹#, Megan Bergkessel¹, Dianne K. Newman^{1,2}#

4

5 ¹Division of Biology and Biological Engineering, California Institute of Technology,
6 Pasadena, CA, USA

7 ²Division of Geological and Planetary Sciences, California Institute of Technology,
8 Pasadena, CA, USA

9

10 Running Title: Aggregation regulation in nontuberculous mycobacteria

11

12 # -corresponding authors dkn@caltech.edu, whdepas@caltech.edu

13

14

15

16

17

18

19 **Abstract:**

20 Nontuberculous mycobacteria (NTM) are emerging opportunistic pathogens that
21 form biofilms in environmental reservoirs such as household water systems and
22 aggregate into phagocytosis-resistant clusters during infection. NTM constitutively
23 aggregate *in vitro*, a phenotype typically considered to be a by-product of the mycolic-
24 acid-rich cell wall. While culturing a model NTM, *Mycobacterium smegmatis*, in rich
25 medium, we fortuitously discovered that planktonic cells accumulated in the culture after
26 ~3 days. By providing selective pressure for bacteria that disperse earlier, we isolated a
27 strain with two mutations in the oligopeptide permease operon (*opp*). A mutant lacking
28 the *opp* operon (Δopp) dispersed earlier and more completely than wildtype (WT). We
29 show that Δopp 's aggregation defect was nutrient related; aggregation was restored by
30 non-peptide carbon sources. Experiments with WT *M. smegmatis* revealed that growth
31 as aggregates is favored when carbon is replete, while dispersal can be induced by
32 carbon starvation. In addition, under conditions of low available carbon relative to
33 available nitrogen, *M. smegmatis* grows as planktonic cells. By adjusting carbon and
34 nitrogen sources in defined medium, we tuned the cellular C:N ratio such that *M.*
35 *smegmatis* grows either as aggregates or planktonic cells. Lastly, we tested the effect of
36 C:N balance on aggregation in clinically relevant NTM. Altogether, we show that NTM
37 aggregation is a controlled process that is regulated by the relative availability of carbon
38 and nitrogen for metabolism. Because NTM aggregation is correlated with increased
39 virulence, these results may contribute to targeted anti-biofilm therapeutics.

40

41 **Importance:**

42 Free-living bacteria can assemble into multicellular aggregates called biofilms.
43 Biofilms help bacteria tolerate multiple stresses, including antibiotics and the host
44 immune system. Differing environmental pressures have resulted in biofilm architecture
45 and regulation varying among bacterial species and strains. Nontuberculous
46 mycobacteria are a group of emerging opportunistic pathogens that utilize biofilms to
47 adhere to household plumbing and showerheads and to avoid phagocytosis by host
48 immune cells. Mycobacteria harbor a unique cell wall built chiefly of long chain mycolic
49 acids that confers hydrophobicity and has been thought to cause constitutive
50 aggregation in liquid media. Here we show that aggregation is instead a regulated
51 process dictated by the balance of available carbon and nitrogen. Understanding that
52 mycobacteria utilize metabolic cues to regulate the transition between planktonic and
53 aggregated cells reveals an inroad to controlling aggregation through targeted
54 therapeutics.

55

56

57

58

59

60

61

62 **Introduction:**

63 The adhesive biofilm matrix can serve as a physical barrier against external
64 stresses such as desiccation and predation, can interact with and sequester
65 antimicrobial agents, and can short-circuit phagocyte signaling (1–4). Additionally, the
66 3D structure of biofilms creates chemical gradients across a cellular population (5–9),
67 resulting in a spectrum of physiologies and metabolisms which, along with genetic
68 diversification and stochastic differences in gene expression, gives rise to substantial
69 cell-to-cell heterogeneity (9–12). Heterogeneous bacterial communities demonstrate
70 increased fitness compared to homogenous communities in a variety of models and
71 experimental systems (11–13). Notably, most antibiotics target rapidly dividing bacteria,
72 so slow-growing and dormant cells that develop in biofilms contribute to antibiotic
73 tolerance (5, 10, 14–17).

74 Nontuberculous mycobacteria (NTM) are emerging pathogens that utilize biofilm
75 formation for survival and persistence both in the host and in the non-host environment
76 (18–22). NTM are adept at surviving standard water decontamination protocols and are
77 commonly found in household water systems, often growing as biofilms (18, 23). NTM
78 can infect healthy adults after repeated exposure and are especially dangerous to
79 immunocompromised populations and patients with lung disorders such as Cystic
80 Fibrosis (CF) and Chronic Obstructive Pulmonary Disease (COPD) (23–26). Infections
81 with NTM can be very difficult to treat; *M. abscessus* lung infections, in particular,
82 require long courses of antibiotic cocktails that have limited efficacy and extensive
83 adverse side effects (24, 27, 28). The ability of *M. abscessus* to aggregate into cord-like
84 aggregates correlates with increased pathogenicity in a zebrafish model and an

85 enhanced ability to evade phagocytosis (19–21), indicating that the formation of
86 multicellular structures by NTM is positively related to their sustained infection of hosts.

87 Bacteria have evolved to enter and exit from the biofilm state in response to
88 species- and strain-specific environmental signals. Peculiarly, mycobacteria form *in vitro*
89 biofilms in nearly all laboratory culture conditions; aggregating into hydrophobic clumps
90 in shaking cultures and forming pellicle biofilms at the air/liquid interface of static
91 cultures (29–32). While environmental parameters such as iron and CO₂ affect
92 mycobacterial pellicle maturation, cues driving the transition between planktonic cells
93 and biofilms have not been identified due to the apparent absence of a true planktonic
94 state (33, 34). Constitutive aggregation suggests either that mycobacteria express
95 adhesive structures in response to signals that are very common in laboratory cultures,
96 or that they have adapted to always grow as aggregates in aqueous environments. The
97 latter possibility has become the dominant paradigm, exemplified by the common
98 addition of detergents such as Tween 80 to mycobacterial cultures to prevent clumping
99 (31, 32).

100 In this study, we set out to understand whether and how aggregation is regulated
101 in NTM. Towards this end, we developed an assay to quantify mycobacterial
102 aggregation in liquid media under varying nutritional environments. Contrary to the
103 conventional wisdom, we found that aggregation and dispersal are regulated processes
104 in a variety of NTM, both pathogenic and non-pathogenic, dictated in large part by the
105 relative availability of carbon and nitrogen.

106

107 **Results:**

108 **Mycobacterial aggregates disperse as cultures age**

109 During routine culture in a rich medium with no detergent, the model NTM
110 *Mycobacterium smegmatis* MC²155 grows as aggregated clumps. However, we noted
111 that non-aggregated (planktonic) cells accumulated after ~40 hours of growth (Fig. 1A).
112 We developed an assay to distinguish and quantify aggregated cells and planktonic
113 cells over time. Briefly, culture replicates were harvested over time by passing an entire
114 culture through a 10 µm cell strainer. The OD₆₀₀ of cells that passed through the strainer
115 (planktonic fraction) was immediately recorded. Aggregates that collected on the
116 strainer were water bath sonicated in PBS + 24.8% Tween 20, and the OD₆₀₀ of the
117 resultant suspension was recorded (Fig. 1B). Phase contrast microscopy revealed that
118 the planktonic fraction was composed mostly of single cells and small clusters (Fig. 1C).
119 SEM of a representative aggregate revealed a densely packed structure (Fig. 1D).
120 Performing this assay on *M. smegmatis* grown in rich medium + 0.2% glucose revealed
121 a decrease in the aggregate fraction concurrent with planktonic cell accumulation after
122 ~40 hours of growth, suggesting a mechanism of controlled dispersal (Fig. 1E).

123 **Mutations in oligopeptide permease genes cause early dispersal**

124 To gain insight into the genetic regulation of *M. smegmatis* aggregation and dispersal,
125 we designed an evolution experiment to select for mutants that disperse earlier than WT
126 in rich medium + 0.2% glucose. Briefly, every 24 hours 1 mL of a 5 mL culture was
127 centrifuged at low speed to pellet aggregates. A new 5 mL culture was inoculated with
128 100 µL of the supernatant and grown for another 24 hours (Fig. 2A). After 60 passages
129 (roughly 575 doublings), planktonic cells visibly accumulated after 24 hours of growth.

130 Passage 60 was plated and a single colony was selected and cultured. The passage 60
131 isolate displayed an early dispersal phenotype compared to WT in rich medium + 0.2%
132 glucose (Fig. 2B). We sequenced the genomes of the passage 60 isolate, our WT strain
133 (passage 0), and a passage 40 isolate that showed no early dispersal phenotype (Fig.
134 S1). In total, the passage 40 isolate had 13 mutations compared to our passage 0
135 isolate, seven of which were in non-transposon open reading frames (ORFs). The
136 passage 60 isolate had 11 mutations compared to our passage 0 isolate, nine of which
137 were in non-transposon ORFs (Table 1).

138 To identify dispersal-related mutations, we narrowed our list of passage 60
139 candidate genes by discarding two genes that were also mutated in the passage 40
140 isolate (MSMEG_2148 and MSMEG_5061), one gene that acquired a silent mutation
141 (MSMEG_3677), and *divIVA* (MSMEG_4217) because it is essential in *M. smegmatis*
142 (35). We generated deletion mutants in a WT background of the four remaining
143 candidates: *oppF*, *oppD*, *kdpD*, and the hypothetical gene MSEM_G_6497. Because
144 *oppF* and *oppD* code for two ATPase subunits associated with an oligopeptide
145 permease (opp) complex, we deleted the entire 5-gene *opp* operon (MSMEG_0643-
146 MSMEG_0639, termed Δopp). While $\Delta kdpD$ and $\Delta MSEM\text{G}_6497$ showed no dispersal
147 phenotype (Fig. S2), Δopp phenocopied the passage 60 isolate by displaying early
148 dispersal (Fig. 2B), indicating that a functional oligopeptide permease system helps
149 maintain aggregation in rich medium + 0.2% glucose.

150 The Opp complex imports oligopeptides for signaling and/or catabolism in
151 multiple bacterial species (36, 37). Our rich medium contains tryptone and yeast extract,
152 both of which are composed largely of oligopeptides, so we reasoned that 1.)

153 exogenous peptides themselves are a pro-aggregation signal, 2.) a self-produced
154 peptide pheromone serves as a pro-aggregation signal, or 3.) metabolizing peptides as
155 nutrients provides the cell with a pro-aggregation signal. To distinguish between these
156 possibilities, we grew WT and Δopp in a defined, peptide-free glycerol medium. If
157 exogenous peptides are necessary for aggregation (1), neither WT nor Δopp should
158 aggregate in the peptide-free medium; if a self-produced pheromone is required for
159 aggregation (2), WT should aggregate but Δopp should be defective; if peptides are
160 used as a nutrient that provides a pro-aggregation signal (3), providing the cells with
161 alternative carbon and nitrogen sources should bypass the need for peptide import and
162 both strains should aggregate. Both WT and Δopp maintained aggregation to a similar
163 degree in glycerol defined medium (Fig. 2C), suggesting that the Opp complex
164 promotes aggregation in rich medium by increasing cells' access to the peptide nutrient
165 sources.

166 **Carbon availability dictates *M. smegmatis* aggregation and dispersal**

167 Because Δopp 's aggregation deficiency in rich medium + 0.2% glucose appeared to be
168 due to a defect in nutrient uptake, we tested whether non-peptide carbon
169 supplementation could complement this defect. Indeed, glucose addition prolonged
170 aggregation in both WT and Δopp , suggesting that carbon starvation is a signal for
171 dispersal (Fig. 3A, Fig S3A). Because of the utility of being able to measure near-
172 complete dispersal, rich medium experiments going forward contain no glucose unless
173 otherwise noted. If carbon starvation leads to aggregate dispersal, we would predict that
174 either carbon-free buffer or carbon-depleted medium should be sufficient to induce
175 dispersal. We therefore resuspended WT aggregates (grown in rich medium for 48

176 hours) in either PBS or conditioned medium from 52-hour-old cultures. After 12 hours,
177 we harvested and quantified aggregated and planktonic populations (Fig. 3B).
178 Aggregates decreased to a similar degree in both conditioned medium and PBS (Fig.
179 3B). Furthermore, when 0.6% glucose was added to conditioned medium, dispersal was
180 largely prevented (Fig. 3B). Unexpectedly, when aggregates were resuspended in
181 conditioned medium, planktonic cells accumulated to a significantly higher extent
182 compared to PBS (Fig. 3B). This result indicated that, instead of growth as aggregates
183 and subsequent dispersal, there may be a window of time in a rich medium culture
184 wherein nutrient conditions favor growth as planktonic cells.

185 **Low C:N ratio drives growth as planktonic cells**

186 Because the OD₆₀₀ has a limited range in which it can accurately measure cell density,
187 we measured CFUs/mL of both aggregated and planktonic fractions over time in rich
188 medium (Fig. 4A). This experiment revealed three distinct phases of growth. In phase I
189 (~0-40 hours), both fractions grow at similar rates with the aggregated fraction
190 outnumbering the planktonic fraction by roughly 10 fold. In phase II (~40-53 hours),
191 planktonic cells continue growing while aggregated fraction growth ceases. Then, in
192 phase III (at ~53 hours onward), aggregates disperse and the planktonic fraction enters
193 stationary phase (Fig. 4A). Our results from Fig. 3 suggest that carbon excess and
194 depletion drive growth as aggregates and aggregate dispersal, respectively. Therefore,
195 we sought to characterize the phase II culture conditions that favored planktonic cell
196 growth. One well-characterized side effect of bacterial growth on peptides is the release
197 of excess ammonium into the medium (38). Indeed, ammonium levels increased as our
198 cultures aged, reaching ~33 mM at 48 hours (Fig. 4B). To test whether ammonium

199 facilitated growth as planktonic cells, we added excess NH₄Cl to starting cultures and
200 tracked aggregation. Ammonium addition led to earlier accumulation of planktonic cells
201 and reduced aggregation (Fig. 4C, S3). To test whether salts have a general effect on
202 aggregation, we added 75 mM NaCl to WT cultures. NaCl did not affect aggregation
203 kinetics, indicating that ammonium specifically favors planktonic growth (Fig. S4). If the
204 high ammonium concentration in conditioned medium favors growth as planktonic cells,
205 it is notable that adding excess carbon to conditioned medium shifts the population back
206 towards growth as aggregates (Fig. 3B). Altogether, these results are consistent with a
207 model wherein carbon replete conditions favor growth as aggregates, high nitrogen
208 (relative to carbon) conditions favor growth as planktonic cells, and carbon depletion
209 leads to aggregate dispersal.

210 **Defined medium designed for growth as aggregated or planktonic cells**

211 To test whether *M. smegmatis* is able to grow as planktonic cells at low C:N ratios, we
212 designed defined medium to supply the bacteria with either replete carbon and low
213 nitrogen (high C:N) or replete nitrogen and low carbon (low C:N). To grow *M.*
214 *smegmatis* with high C:N availability, we used glycerol as the main carbon source,
215 glutamate as the main nitrogen source, and no ammonium (117 mM carbon, 5.5 mM
216 nitrogen, C:N of the medium = 21.4). Glycerol is commonly supplied to mycobacteria
217 because it supports fast growth and, as a small (three-carbon) uncharged molecule, can
218 presumably passively diffuse across the mycolic acid barrier (39). Indeed, growth on
219 glycerol floods most central metabolite pools compared to growth on other carbon
220 sources in *Mycobacterium tuberculosis* (40). To generate low C:N availability, we used
221 a charged three-carbon compound, pyruvate, as the main carbon source, and added 20

222 mM NH₄Cl in addition to glutamate as the nitrogen source (117 mM carbon, 25.5 mM
223 nitrogen, C:N of the medium = 4.58). In some bacteria, the relative availability of carbon
224 and nitrogen sources can be reflected in total C:N content of the cell (41). Therefore, to
225 assess whether our medium was effectively providing high or low C:N availability, we
226 directly measured the ratio of cellular carbon to cellular nitrogen (by mass) of *M.*
227 *smegmatis* grown in either pyruvate or glycerol medium when the total OD₆₀₀ was
228 between 0.5 and 0.7. As predicted, *M. smegmatis* grown on glycerol had a C:N ratio of
229 6.95, (stdev 0.85), and on pyruvate + NH₄Cl had a C:N ratio of 5.02 (stdev 0.31, p =
230 0.005). Consistent with our hypothesis, *M. smegmatis* grew mostly as aggregates on
231 glycerol and grew mostly as planktonic cells on pyruvate (Fig. 5A,B).

232 The ratio of C:N in natural environments such as soil affects bacterial diversity
233 and growth and is often tuned in order to favor desired bacterial metabolisms in
234 industrial settings (42, 43). It is therefore notable that even when grown in pyruvate
235 defined medium with no ammonium (117 mM carbon, 5.5 mM nitrogen, C:N of the
236 medium = 21.4, equal to glycerol defined medium), *M. smegmatis* had a relatively low
237 cellular C:N ratio of 5.23 (stdev 0.38, p = 0.01 compared to glycerol grown cells) and
238 grew as mostly planktonic cells (Fig. S5). These results reinforce that the form of
239 available nutrients, and not just total carbon and nitrogen in an environment, can impact
240 a cell's C:N status and dependent phenotypes.

241 Lastly, we leveraged our pyruvate defined medium to test whether planktonic
242 cells can transition to aggregates. Planktonic *M. smegmatis* was grown for 36 hours in
243 pyruvate + NH₄Cl defined medium before addition of 0 or 25 mM glycerol. By six hours
244 post glycerol addition, the majority of the planktonic population had aggregated (Fig.

245 5C), further demonstrating that aggregation state is dynamic and dependent on the ratio
246 of available C:N.

247 **C:N-dependent aggregation regulation is common among NTM**

248 To determine whether C:N regulation of aggregation is conserved among clinically
249 relevant NTM, we grew type strains of *M. abscessus* and *M. fortuitum* along with four *M.*
250 *abscessus* subsp. *abscessus* clinical isolates (two rough colony isolates and two
251 smooth colony isolates) in rich medium and tracked aggregation kinetics (Fig. 6, S6).

252 Both type strains and one smooth colony clinical isolate accumulated planktonic cells at
253 later culture timepoints, with glucose addition increasing total aggregation and
254 ammonium addition favoring growth as planktonic cells (Fig. 6, S6). Neither rough
255 colony *M. abscessus* isolate accumulated planktonic cells, even after addition of
256 ammonium. In contrast, the smooth colony isolate that did not disperse in rich medium
257 grew solely as planktonic cells when provided with supplemental ammonium.

258 Altogether, our results indicate that C:N balance is a common regulator of NTM
259 aggregation, with rough colony clinical isolates being a possible exception.

260

261 **Discussion:**

262 The role of biofilm formation in rendering bacteria recalcitrant to antibiotics and
263 immune killing provides motivation to develop novel anti-biofilm strategies. However,
264 because bacteria have evolved to occupy and form biofilms in diverse ecological niches,
265 the regulatory pathways and physical components that govern biofilm formation differ
266 significantly between species. As such, a species-specific, in-depth understanding of
267 how cells sense and respond to their environment by aggregating under certain

268 conditions, and growing as planktonic cells under others, is essential in order to control
269 bacterial biofilm formation for any specific pathogen. In this work, we have found a role
270 for C:N balance in dictating the transition between planktonic and aggregated states in
271 NTM.

272 Understanding the environmental niches in which NTM have evolved can lend
273 context to our finding that C:N balance controls aggregation state. NTM are non-motile
274 saprophytes that are common residents of soil and waterways (22, 28, 44). In soil,
275 carbon is most often the limiting nutrient for bacterial growth (45, 46). At a low C:N ratio,
276 our data suggest that NTM could exist at least partly as planktonic cells. As water flow is
277 a major factor in determining movement of bacteria through soil (47, 48), NTM in this
278 state might be susceptible to water-mediated transport to another region of the
279 rhizosphere (potentially containing more carbon). Larger bacterial cell sizes correlate
280 with decreased movement through soil (49). Therefore, if NTM were growing as
281 aggregates in carbon-rich conditions, we would expect them to be less likely to be
282 washed away into potentially more carbon-depleted regions. While speculative, this
283 natural ecological context motivates us to consider how mycobacteria might sense the
284 C:N balance in their environment and control their aggregation state accordingly.

285 It is well appreciated that carbon and nitrogen availability dictate the metabolic
286 and growth capacity of a cell (50, 51), and bacteria are able to coordinate carbon and
287 nitrogen metabolism through a variety of means (52). The cellular C:N ratio provides a
288 rough estimate of the cell's C:N status, but it is not a parameter that a cell can directly
289 sense. How then do mycobacteria translate C:N availability to aggregation? Our data
290 show that no one carbon source is necessary to drive aggregation. Interestingly, by

291 responding to flux through a metabolic pathway, a cell can integrate the signal from
292 multiple inputs without needing to measure each one specifically (53). It thus seems
293 possible that mycobacteria sense and respond to flux-dependent metabolites –
294 molecules whose intracellular pools correlate with flux through specific metabolic
295 pathways, such as fructose-1,6-bisphosphate (FBP), the levels of which correlate with
296 glycolytic flux (53, 54), or 2-oxoglutarate (2OG), the levels of which correlate to flux
297 through the TCA cycle (53, 55). Alternatively, or in addition, two-component systems
298 might mediate the translation between metabolite availability and aggregation.
299 Uncovering the pathways through which NTM achieve aggregation control is a priority
300 for future work.

301 Regardless of the signal transduction mechanism, a surface adhesin must
302 mediate the aggregation phenotype. Like many members of the *Corynebacteriales*
303 order, mycobacteria produce a mycomembrane: a cell wall composed of peptidoglycan,
304 arabinogalactan covalently linked to an inner leaflet of long-chain mycolic acids, and an
305 outer layer of extractable lipids, lipoglycans, and proteins (56, 57). As such, the
306 mycobacterial cell wall is unusually lipid rich (58, 59). A lipid-rich cell wall fits the long-
307 standing observation that mycobacteria clump together into hydrophobic aggregates; in
308 his original description of *M. tuberculosis* in 1882, Robert Koch noted that the bacteria
309 “...ordinarily form small groups of cells which are pressed together and arranged in
310 bundles” (60). Clumping (or cording, depending on aggregate morphology) is now
311 recognized as a ubiquitous feature of pathogenic and nonpathogenic mycobacteria (21,
312 32, 61). As clumps are hydrophobic, detergents such as Tween 80 are almost

313 universally added to mycobacterial cultures to favor growth as dispersed cells (32, 61,
314 62).

315 Inherent to the chemical intuition linking a lipid-rich cell wall and spontaneous
316 clumping is the assumption that mycobacteria display a *constitutively hydrophobic* cell
317 surface. Several studies of the mycomembrane composition challenge this dogma.

318 Trehalose dimycolate (TDM) was originally called ‘cord factor’ because cording is
319 reduced when TDM is removed from the cell envelope via petroleum ether extraction
320 (63–65). TDM expression is regulated by sugar availability in *M. avium*, implying that
321 TDM-mediated aggregation can be controlled by the cell in response to the environment
322 (66). Likewise, mycolic acid chain length affects aggregation (67), and *M. smegmatis*
323 can regulate mycolic acid chain length in response to environmental factors (29, 68).

324 Finally, genes involved in the biosynthesis and glycosylation of cell-surface
325 glycopeptidolipids (GPLs) in *M. smegmatis*, *M. avium*, and *M. abscessus* affect
326 aggregation and cell surface hydrophobicity (69–72). GPL production and glycosylation
327 are also regulated by chemical signals (70, 73). In addition to providing evidence that
328 mycobacteria can dynamically regulate cell envelope composition and surface
329 hydrophobicity, these studies provide candidate adhesins that could be effectors of C:N-
330 driven aggregation regulation.

331 Finally, the fact that NTM regulate aggregation has potentially important
332 biomedical relevance. New treatments are needed to combat NTM infections, such as
333 those caused by *M. abscessus*, which is notoriously difficult to eradicate. It is
334 noteworthy that rough colony isolates of *M. abscessus* subsp. *abscessus* do not
335 disperse in rich medium. Rough *M. abscessus* isolates are typically the result of

336 mutations that reduce GPL production (72, 74, 75). Accordingly, we might hypothesize
337 that C:N regulation is linked to GPL production or modification, which directly impacts
338 the aggregation state. It is worth exploring whether nodes along such a pathway could
339 be identified and exploited as new targets for biofilm control. The rising threat of NTM
340 infections, particularly to susceptible communities such as CF patients, as well as the
341 correlation between increased aggregation and virulence, lends motivation to further
342 probe the mechanisms of aggregation and dispersal in these pathogens (19, 21, 27,
343 28).

344

345

346

347

348

349

350

351

352

353

354

355

356

357

358

359 **Materials and Methods:**

360 **Strains and growth conditions –** Strains, plasmids, and primers used in this study are
361 listed in table S1. The rich medium used in this study was TYEM (10 g tryptone, 5 g
362 yeast extract/L + 2 mM MgSO₄). Where noted, filter sterilized glucose or NH₄Cl were
363 added as supplements to autoclaved TYEM. For routine culturing of mycobacteria,
364 bacteria were grown in TYEM for ~50-70 hours, at which time cultures were passed
365 through 10 µm strainers (from pluriSelect, 43-50010-03) and planktonic cells were
366 collected and processed. The exception was rough *M. abscessus* isolates NTM0253b
367 and NTM0711b, which were cultured in TYEM + 0.05% Tween 80. Our defined medium
368 was modified M63 -- 13.6 g KH₂PO₄ was dissolved in 500 mL Nanopure H₂O and the
369 pH was adjusted to 7.0 via addition of KOH. This 2X stock was filter sterilized and
370 diluted to 1X with Nanopure H₂O while adding filter sterilized supplements: MgSO₄ to 1
371 mM, FeSO₄ to 10 uM, SL-10 trace metal solution to 1x, proline to 0.5 mM, sodium
372 glutamate to 5 mM, NH₄Cl to 20 mM (when noted), and either glycerol to 30 mM or
373 sodium pyruvate to 30 mM. Mutants in *M. smegmatis* MC²155 were made via
374 recombineering as described with minor alterations (76). Briefly, *M. smegmatis*
375 transformed with pJV53 was grown in TYEM + 0.05% Tween 80 + 25 ug/mL kanamycin
376 until it reached an OD₆₀₀ of 0.4-0.5. Acetamide was added to 0.2% and cells were
377 incubated for 3 hours shaking at 250 rpm at 37°C. Cells were then made
378 electrocompetent by serial washes with chilled 10% glycerol (1/2, 1/10th, 1/20th, 1/100th
379 original volume) with centrifugation at 4000 xg for 10 minutes at 4°C between washes.
380 100 uL of the cell mixture was then electroporated with 200 ng of linear DNA encoding a
381 gentamicin resistance cassette (PCR amplified from plasmid pMQ30) flanked by 400-

382 500 bps of sequence upstream and downstream of the target genes. Flanking regions
383 were PCR-amplified from WT *M. smegmatis* colonies and Gibson assembly was utilized
384 to combine flanking regions with the gentamicin resistance cassette. After mutagenesis,
385 mutant strains were cured of pJV53 by passaging on TYEM with no antibiotics 3-7 times
386 until they were verified as kanamycin-sensitive.

387 **Light microscopy and SEM**

388 For light microscopy, samples were loaded onto Tekdon poly-L-lysine coated slides and
389 phase contrast images were acquired on a Zeiss AxioObserver.A1 using a 40x 1.3 NA
390 oil immersion objective. For SEM, WT *M. smegmatis* was grown in rich medium for 24
391 hours, at which point the culture was passed through a 10 µm strainer and washed with
392 PBS. Aggregates that collected on the strainer were fixed in 4% PFA for 2 hours at
393 room temperature, washed 2x with PBS, and fixed in 1% OsO₄ for 1 hour at room
394 temperature. After two more rinses with PBS, aggregates were dehydrated in an
395 ethanol series, with 10 minute incubations in 50%, 70%, 90%, 95%, 100% ethanol, and
396 a final incubation in 100% ethanol for 1 hour. Samples were then incubated in a 1:2
397 solution of hexamethyldisilazane (HMDS):ethanol for 20 minutes, a 2:1 solution of
398 HMDS:ethanol for 20 minutes, followed by two incubations in 100% HMDS for 20
399 minutes each. Samples were then loaded onto silicon wafers, air dried, and attached to
400 imaging stubs with conductive tape. Samples were sputter coated with 10 nm of
401 palladium and imaged on a Zeiss 1550VP field emission SEM using an SE2 detector.

402 **Aggregation assays**

403 Medium for aggregation assays was prepared in flasks and inoculated with the indicated
404 strain of bacteria to an OD₆₀₀ of 0.01. After mixing, 5 mL aliquots were pipetted into

405 brand-new borosilicate disposable culture tubes. These culture replicates were
406 incubated at 37°C while shaking at 250 rpm. At indicated timepoints, a single culture
407 replicate was harvested by pouring the entire culture through a 10 µm strainer. Culture
408 that passed through the strainer was designated as the planktonic cell fraction and the
409 OD₆₀₀ was immediately recorded. The original culture tube was washed with 5 mL of
410 PBS, which was then poured over the aggregate fraction to remove residual planktonic
411 cells. Aggregates that remained on the strainer were resuspended in 4.5 mL PBS + 6%
412 Tween 20 and poured back in the original culture tube. 500 µL of Tween 20 was added
413 for a final volume of 5 mLs and a final Tween 20 concentration of 28.5%. Aggregate
414 fractions were then water bath sonicated until no visible clumps remained, and the
415 OD₆₀₀ of the aggregate fraction was recorded. For CFU counts, a slightly modified
416 protocol was employed for the aggregate fraction. Instead of PBS, aggregates were
417 resuspended in TYEM + 0.05% Tween 80, to which 100 µL of autoclave-sterilized
418 Tween 20 was added. Aggregates were then water bath sonicated until no clumps were
419 visible. Both planktonic and aggregate fractions were then serially diluted in TYEM +
420 0.05% Tween 80 and serial dilutions spanning seven orders of magnitude were plated
421 on TYEM agar plates as 10 µL drips. Plates were incubated at 37°C for ~2 days and
422 colonies were counted at the appropriate dilution. Conditioned medium was prepared by
423 centrifuging 52-hour-old cultures and filtering the supernatant through a 0.2 µm filter.
424 For conditioned medium experiments, three 48-hour-old cultures were pooled by
425 passing them through a single 10 µm strainer. Aggregates were washed with 5 mL of
426 PBS and then resuspended in 15 mL of conditioned medium (or PBS as indicated). 5

427 mL aliquots were partitioned into three culture tubes, and after 12 hours of shaking at
428 37°C, aggregates and planktonic cells were separated and quantified.

429 **Evolution Experiment/Sequencing**

430 WT *M. smegmatis* was inoculated into TYEM + 0.2% glucose. After 24 hours, 1 mL of
431 culture was centrifuged for 1 minute at 2000 x g. 100 µl of supernatant was inoculated
432 into a new TYEM + 0.2% glucose culture. The process was repeated every 24 hours.
433 After 60 passages, planktonic cells were visibly accumulating at 24 hours. This culture
434 was plated on TYEM agar plates and a single colony was selected as the passage 60
435 isolate. Along with an isolate from passage 0 and passage 40, this strain was grown to
436 mid-exponential phase and DNA was extracted as described (77). DNA was fragmented
437 using the NEBNext dsDNA Fragmentase (New England Biolabs, Ipswich MA) according
438 to the manufacturer's instructions. Briefly, 1 µg of passage 0 and passage 40 DNA and
439 725 ng of passage 60 DNA were treated with fragmentase for 15 minutes in order to
440 achieve an acceptable size distribution, which was assessed using a High-Sensitivity
441 DNA chip on a Bioanalyzer instrument (Agilent). Libraries for sequencing were prepared
442 using the NEBNext DNA Library Prep kit according to instructions, which included end-
443 repair of the fragments, dA-tailing, and ligation to adaptors. Each sample was PCR-
444 amplified with a universal primer and a unique bar-coded primer, using 12 amplification
445 cycles. Final libraries were verified using a Bioanalyzer High-Sensitivity DNA chip and
446 quantified using the Qubit fluorimeter and dsDNA dye (Invitrogen). Sequencing was
447 performed by the Millard and Muriel Jacobs Genetics and Genomics Laboratory at the
448 California Institute of Technology using the Illumina HiSeq 2500 platform. Approximately
449 15 million single reads of 50 bp each were collected for each sample. Base-calling and

450 de-multiplexing were performed by the Illumina HiSeq Control Software (HCS, version
451 2.0). The resulting FASTQ files were concatenated into one file per sample and filtered
452 and trimmed by quality score per base using the Trimmomatic software package with
453 the following parameters: LEADING:27 TRAILING:27 SLIDINGWINDOW:4:20
454 MINLEN:35 (78). Surviving reads were mapped to the *Mycobacterium smegmatis* str.
455 MC2 155 genome (gi|118467340|ref|NC_008596.1) using bwa (version 0.7.12) (79),
456 and sorted and converted to binary format using SAMtools (version) (80). Tools from
457 the Genome Analysis Tool Kit (GATK, version 2.7-4-g6f46d11) (81) were used to call
458 SNPs and small insertions and deletions relative to the reference genome as follows:
459 first, duplicate reads were identified and marked using the MarkDuplicates tool. Next,
460 putative insertions and deletions were identified using the RealignerTargetCreator tool,
461 and reads surrounding them were re-aligned using the IndelRealigner tool. Finally,
462 putative variants relative to the reference genome were called using the
463 UnifiedGenotyper tool. 144 variant regions were confidently identified in the passage 0
464 sample, 153 variant regions were identified in the passage 40 sample, and 154 variant
465 regions were identified in the passage 60 sample. Most of these variations were
466 common to all three samples and were not considered further. For mutations of interest,
467 the effects on protein coding sequence were predicted using the snpEff tool (version
468 SnpEff 4.3t) (82). Genes affected by variations in non-transposon ORFs arising in the
469 passage 40 and passage 60 sample relative to the passage 0 sample are listed in table
470 1.

471 **Ammonium measurements**

472 At the time points indicated, 1 mL of culture was centrifuged at 16,000 × g at room
473 temperature for 1 minute to pellet cells. Supernatants were filter sterilized through a 0.2
474 µm syringe filter and diluted 1:40 in nanopure H₂O. Parallel ion chromatography
475 systems operated simultaneously (Dionex ICS 200, Environmental Analysis Center,
476 Caltech) were used to measure ammonium. A single autosampler (Dionex AS 40)
477 loaded both systems' sample loops serially. The 5 µL sample loop on the anion IC
478 system was loaded first, followed by a 5 µL sample loop on the cation IC system. Both
479 columns and both detectors were maintained at 30°C. Anionic components in the
480 sample were resolved using a AS-19 separator (2x250mm) column protected by an AG-
481 19 guard (2x50mm). A hydroxide gradient was produced using a potassium hydroxide
482 eluent generator cartridge and pumped at 0.25 mL per minute. The gradient began with
483 a 10 mM hold for 10 minutes, increased linearly to 58 mM at 25 minutes, remaining at
484 58 mM until the end of data acquisition at 32 minutes. Seven minutes were allowed
485 between analyses to return the column to initial conditions. Anions were detected at
486 neutral pH using an AERS - 500 2mm suppressor (Thermo) operated in eluent recycle
487 mode with an applied current of 30 mA and conductivity detection cell maintained at
488 35°C. A carbonate removal device (CRD 200 2mm) was installed between the
489 suppressor eluent out and the conductivity detector eluent in ports. Ammonium,
490 calcium, magnesium, potassium and sodium were resolved using a CS-12A separator
491 column (2x250mm) protected by a CG-12A guard column (2x50). Isocratic
492 methylsulfonate at 20 mM was produced using a methylsulfonic acid based eluent
493 generated cartridge and pumped at 0.25 mL per minute. Suppressed conductivity
494 detection using a Dionex CERS-500 2 mm suppressor operated in eluent recycle mode

495 with an applied current of 15 mA. Ammonium standards ranging from 1 μ M to 1 mM (1
496 μ M, 10 μ M, 50 μ M, 100 μ M, 500 μ M, and 1 mM) were run along with samples. A
497 standard curve was generated by fitting a quadratic curve to standard measurements.

498 **C:N measurements**

499 For defined medium conditions, 16 5 mL cultures (either in pyruvate defined medium +/-
500 NH₄Cl or glycerol defined medium) were grown to an OD₆₀₀ between 0.5 and 0.7. The
501 16 cultures were divided into two sets of eight cultures. All eight cultures in a set were
502 poured into a single 50 mL conical tube. Samples were then centrifuged at 6000 x g for
503 10 minutes at 4°C. Pellets were then washed 2x with 25 mL PBS, with centrifugation in
504 between. After the second wash, each pellet was resuspended in 1.2 mL PBS, which
505 was divided among two 1.5 mL centrifuge tubes in 600 μ L aliquots (for a total of four
506 samples/condition). After centrifugation at 16000 x g for 1 minute, supernatants were
507 pipetted off and pellets were flash frozen in liquid nitrogen and stored at -80°C. Frozen
508 samples were lyophilized, and ~50 μ g (for carbon measurement) and ~700 μ g (for
509 nitrogen measurement) of each sample was weighed into an OEA lab tin capsule
510 (pressed, ultra-clean, C61480.096P). Carbon and nitrogen were measured separately
511 due to differing sensitivities of the instrument. Each sample was combusted in a Thermo
512 Fisher EA IsoLink combustion system by oxidation at 1020°C over tungstic oxide,
513 followed by reduction over elemental copper packed in the same furnace. The
514 generated CO₂ and N₂ carried by a continuous helium flow (100ml/min) were
515 subsequently passed through a water trap and then a 5 Å molecular sieve GC at 50°C.
516 The GC was used to separate N₂ from CO₂. Carbon and nitrogen were then diluted with
517 helium in a Conflo IV interface/open split prior to entering the Thermo Fisher Delta V

518 IRMS system for analysis. Depending on the configurations of the IRMS, either CO₂ or
519 N₂ was measured for its total abundance. Integrated peak areas for both CO₂ and N₂
520 were calibrated by running urea standards, and empty tins were included as blanks. A
521 Student's T-test was used to generate p-values comparing conditions.

522

523

524

525

526

527

528

529

530

531

532

533

534

535

536

537

538

539

540

541 **Acknowledgements:**

542 We thank the Cystic Fibrosis Foundation (grants DEPAS17F0 to W.H.D. and
543 BERGKE16F0 to M.B.) and the N.I.H (grant 1R01AI127850-01A1 to D.K.N.) for
544 supporting our research. Lindsay Caverly (CS Mott Children's Hospital, University of
545 Michigan, Ann Arbor, MI, USA) graciously provided *M. abscessus* clinical isolates
546 (NTM0253a, NTM0253b, NTM0711a, and NTM0711b), William Jacobs (Albert Einstein
547 College of Medicine, Bronx, NY, USA) provided WT *M. smegmatis* MC²155, and William
548 Bishai (Johns Hopkins University School of Medicine, Baltimore, MD, USA) provided
549 plasmid pJV53. Igor Antoshechkin and the Millard and Muriel Jacobs Genetics and
550 Genomics Laboratory at Caltech assisted with genome sequencing. Alex Sessions and
551 Fenfang Wu (Caltech) helped with C:N measurements and analysis. Ion
552 chromatography instrumentation used for this work is located in the Environmental
553 Analysis Center at Caltech. We acknowledge Nathan F. Dalleska, Lev Tsypin, and
554 Melanie Spero for Ion Chromatography method support. SEM was performed at the
555 Caltech GPS Division Analytical Facility with the assistance of Chi Ma.

556

557

558

559

560

561

562

563 **Figure Legends:**

564 **Figure 1 – Quantification of mycobacterial aggregation/dispersal over time**

565 (A) In rich medium + 0.2% glucose, *M. smegmatis* grows as clumps at early time points (left
566 tube, 30 hours of growth). In older cultures, planktonic cells accumulate (right tube, 72 hours of
567 growth). (B) Cartoon depicting a method to separate and quantify aggregated and planktonic
568 mycobacterial cells. (C) Phase-contrast micrograph showing the planktonic (top panel) and
569 aggregated (bottom panel) fraction of a 72-hour-old culture. The planktonic fraction is largely
570 single cells and small clumps. Cells that are retained on the strainer (aggregated fraction)
571 mostly exist as large clumps. (D) SEM of a representative *M. smegmatis* aggregate that was
572 retained on the strainer after ~30 hours of growth in rich medium. (E) Aggregation curve of WT
573 *M. smegmatis* grown in rich medium + 0.2% glucose. Cells were harvested at each indicated
574 timepoint and processed with the method outlined in Fig. 1B. Data are representative of n=4
575 trials.

576 **Figure 2 – Mutations in an oligopeptide permease operon lead to early dispersal**

577 (A) Cartoon depicting an evolution experiment to select for an *M. smegmatis* strain that
578 disperses earlier than WT. (B) Aggregation curve of WT *M. smegmatis*, the passage 60 isolate,
579 and Δopp grown in rich medium + 0.2% glucose. The top panel shows the aggregated fraction
580 and the bottom panel shows the planktonic fraction. Data are representative of n=3 trials. (C)
581 Aggregation curve of WT *M. smegmatis* and Δopp grown in glycerol defined medium. The top
582 panel shows the aggregated fraction and the bottom panel shows the planktonic fraction. Data
583 are representative of n=2 trials.

584 **Figure 3 – Carbon depletion leads to dispersal**

585 (A) Aggregation curve of WT *M. smegmatis* in rich medium + no glucose, 0.2% glucose, or 0.6%
586 glucose. The top panel shows the aggregated fraction and the bottom panel shows the
587 planktonic fraction. Data are representative of n=3 trials. (B) Aggregates harvested from 48-
588 hour-old rich medium cultures (Time 0) were resuspended in conditioned medium (filter-
589 sterilized from 52-hour-old-rich medium cultures), PBS, or conditioned medium + 0.6% glucose
590 and grown for 12 hours. Each bar is an average of biological triplicates and error bars represent
591 standard deviation. Asterisks represents p <0.05 by the Student's T-test.

592 **Figure 4 – Low C:N availability favors growth as planktonic cells**

593 A.) CFUs/mL for WT *M. smegmatis* grown in rich medium (no glucose). Each data point is the
594 average of biological triplicates and error bars represent standard deviation. Roman numerals
595 denote three phases of growth as described in text. B.) Aggregation curve of WT *M. smegmatis*
596 in rich medium (no glucose). At indicated time points, three additional cultures were harvested
597 for NH₄ IC measurements. Each NH₄ data point is an average of biological triplicates and error
598 bars represent standard deviation. Aggregation curve data are representative of n=5 trials. C.)
599 Aggregation curve of WT *M. smegmatis* in rich medium (no glucose) with no NH₄Cl, 25 mM
600 NH₄Cl, or 75 mM NH₄Cl. The top panel shows the aggregated fraction and the bottom panel
601 shows the planktonic fraction. Data are representative of n=3 trials.

602 **Figure 5 – Defined medium designed to favor growth as aggregates or planktonic cells**

603 (A) Aggregation curve of WT *M. smegmatis* in glycerol defined medium. Culture image was
604 taken after 27 hours of growth. Data are representative of n=4 trials. (B) Aggregation curve of
605 WT *M. smegmatis* in pyruvate defined medium. Culture image was taken after 34 hours of
606 growth. Data are representative of n=4 trials. (C) WT *M. smegmatis* was grown in pyruvate +
607 NH₄Cl minimal medium for 34 hours (Time 0). Glycerol was then added to 25 mM, and cultures

608 were incubated for six more hours before harvesting. Bars represent biological triplicates and
609 error bars represent standard deviation. Asterisks represents p <0.05 by the Student's T-test.

610 **Figure 6 – C:N regulation of aggregation/dispersal is common among NTM**

611 Aggregation curves in rich medium +/- 0.2% glucose (left column) or rich medium +/- 75 mM
612 NH₄Cl (right column) were recorded for indicated strains. Ten timepoints were selected from
613 each curve to span the entire timecourse. The OD₆₀₀ value of the planktonic fraction was
614 multiplied by -1, and then the OD₆₀₀ values of both fractions were added together. The darkest
615 blue color corresponds to sums of 2.5 or greater and the darkest yellow color corresponds to
616 sums of -2.5 or less. Times are rounded up to the nearest hour. Data are representative of at
617 least n=2 trials. The *M. smegmatis* heatmaps represent aggregation curves shown in Fig. 3A
618 and Fig. 4C. The aggregation curves from which the other heatmaps were derived are included
619 in Fig. S6.

620 **Figure S1 – Passage 40 isolate displays no aggregation defect**

621 Aggregation curve of passage 0 (WT), 40, and 60 isolate in rich medium + 0.2% glucose. The
622 top panel shows the aggregated fraction and the bottom panel shows the planktonic fraction.
623 Data are representative of n=2 trials.

624 **Figure S2 – Neither ΔkdpD (MSMEG_5395) nor ΔMSMEG_6497 have aggregation defects**

625 Aggregation curve of WT, ΔkdpD (MSMEG_5395), and ΔMSMEG_6497 in rich medium + 0.2%
626 glucose. The top panel shows the aggregated fraction and the bottom panel shows the
627 planktonic fraction. Data are representative of n=2 trials.

628 **Figure S3 – Response of Δopp to glucose or ammonium**

629 (A) Aggregation curve of Δopp in rich medium + no glucose, 0.2% glucose, or 0.6% glucose.
630 The top panel shows the aggregated fraction and the bottom panel shows the planktonic
631 fraction. Data are representative of n=2 trials. (B) Aggregation curve of Δopp in rich medium +
632 no glucose with no NH₄Cl, 25 mM NH₄Cl, or 75 mM NH₄Cl. The top panel shows the aggregated
633 fraction and the bottom panel shows the planktonic fraction. Data are representative of n=2
634 trials.

635 **Figure S4 – NaCl does not affect aggregation**

636 Aggregation curve of WT in rich medium (no glucose) with or without 75 mM NaCl. The top
637 panel shows the aggregated fraction and the bottom panel shows the planktonic fraction. Data
638 are representative of n=3 trials.

639 **Figure S5 – Growth as planktonic cells in pyruvate defined medium with no NH₄Cl**

640 Aggregation curve of WT in pyruvate defined medium (with no N₄Cl). Data are representative of
641 n=3 trials.

642 **Figure S6 – C:N regulation of aggregation/dispersal is common among NTM**

643 Aggregation curves of *M. abscessus* ATCC 19977, *M. fortuitum* ATCC 6841, two smooth colony
644 *M. abscessus* subsp. *abscessus* isolates (NTM0253a and NTM0711a), and two rough colony *M.*
645 *abscessus* subsp. *abscessus* isolates (NTM0253b and NTM0711b). Strains were grown in rich
646 medium +/- 0.2% glucose (top row in each panel) and in rich medium (no glucose) +/- 75 mM
647 NH₄Cl (bottom row in each panel). Data are representative of at least n=2 trials.

648

649 Bibliography

- 650 1. **DePas WH, Syed AK, Sifuentes M, Lee JS, Warshaw D, Saggar V, Csankovszki G, Boles BR, Chapman MR.** 2014. Biofilm formation protects *Escherichia coli* against killing by *Caenorhabditis elegans* and *Myxococcus xanthus*. *Appl. Environ. Microbiol.* **80**:7079–7087.
- 654 2. **White AP, Gibson DL, Kim W, Kay WW, Surette MG.** 2006. Thin aggregative fimbriae and cellulose enhance long-term survival and persistence of *Salmonella*. *J. Bacteriol.* **188**:3219–3227.
- 657 3. **Hall CW, Mah T-F.** 2017. Molecular mechanisms of biofilm-based antibiotic resistance and tolerance in pathogenic bacteria. *FEMS Microbiol. Rev.* **41**:276–301.
- 659 4. **Thurlow LR, Hanke ML, Fritz T, Angle A, Aldrich A, Williams SH, Engebretsen IL, Bayles KW, Horswill AR, Kielian T.** 2011. *Staphylococcus aureus* biofilms prevent macrophage phagocytosis and attenuate inflammation *in vivo*. *J. Immunol.* **186**:6585–6596.
- 663 5. **Williamson KS, Richards LA, Perez-Osorio AC, Pitts B, McInerney K, Stewart PS, Franklin MJ.** 2012. Heterogeneity in *Pseudomonas aeruginosa* biofilms includes expression of ribosome hibernation factors in the antibiotic-tolerant subpopulation and hypoxia-induced stress response in the metabolically active population. *J. Bacteriol.* **194**:2062–2073.
- 668 6. **Wessel AK, Arshad TA, Fitzpatrick M, Connell JL, Bonnecaze RT, Shear JB, Whiteley M.** 2014. Oxygen limitation within a bacterial aggregate. *MBio* **5**:e00992.
- 670 7. **DePas WH, Hufnagel DA, Lee JS, Blanco LP, Bernstein HC, Fisher ST, James GA, Stewart PS, Chapman MR.** 2013. Iron induces bimodal population development by *Escherichia coli*. *Proc. Natl. Acad. Sci. USA* **110**:2629–2634.
- 673 8. **Dietrich LEP, Okegbe C, Price-Whelan A, Sakhtah H, Hunter RC, Newman DK.** 2013. Bacterial community morphogenesis is intimately linked to the intracellular redox state. *J. Bacteriol.* **195**:1371–1380.
- 676 9. **Stewart PS, Franklin MJ.** 2008. Physiological heterogeneity in biofilms. *Nat. Rev. Micro.* **6**:199–210.
- 678 10. **Bergkessel M, Basta DW, Newman DK.** 2016. The physiology of growth arrest: uniting molecular and environmental microbiology. *Nat. Rev. Micro.* **14**:549–562.
- 680 11. **Veening J-W, Smits WK, Kuipers OP.** 2008. Bistability, epigenetics, and bet-hedging in bacteria. *Annu. Rev. Microbiol.* **62**:193–210.

- 682 12. **Van Boxtel C, van Heerden JH, Nordholt N, Schmidt P, Bruggeman FJ.** 2017. Taking
683 chances and making mistakes: non-genetic phenotypic heterogeneity and its
684 consequences for surviving in dynamic environments. *J. R. Soc. Interface* **14**.
- 685 13. **Boles BR, Thoendel M, Singh PK.** 2004. Self-generated diversity produces “insurance
686 effects” in biofilm communities. *Proc. Natl. Acad. Sci. USA* **101**:16630–16635.
- 687 14. **Stewart PS.** 2002. Mechanisms of antibiotic resistance in bacterial biofilms. *Int. J. Med.
688 Microbiol.* **292**:107–113.
- 689 15. **Walters MC, Roe F, Bugnicourt A, Franklin MJ, Stewart PS.** 2003. Contributions of
690 antibiotic penetration, oxygen limitation, and low metabolic activity to tolerance of
691 *Pseudomonas aeruginosa* biofilms to ciprofloxacin and tobramycin. *Antimicrob. Agents
692 Chemother.* **47**:317–323.
- 693 16. **Høiby N, Bjarnsholt T, Givskov M, Molin S, Ciofu O.** 2010. Antibiotic resistance of
694 bacterial biofilms. *Int. J. Antimicrob. Agents* **35**:322–332.
- 695 17. **Spero MA, Newman DK.** 2018. Chlorate Specifically Targets Oxidant-Starved, Antibiotic-
696 Tolerant Populations of *Pseudomonas aeruginosa* Biofilms. *MBio* **9**.
- 697 18. **Feazel LM, Baumgartner LK, Peterson KL, Frank DN, Harris JK, Pace NR.** 2009.
698 Opportunistic pathogens enriched in showerhead biofilms. *Proc. Natl. Acad. Sci. USA*
699 **106**:16393–16399.
- 700 19. **Bernut A, Herrmann J-L, Kissa K, Dubremetz J-F, Gaillard J-L, Lutfalla G, Kremer L.**
701 2014. *Mycobacterium abscessus* cording prevents phagocytosis and promotes abscess
702 formation. *Proc. Natl. Acad. Sci. USA* **111**:E943–52.
- 703 20. **Haloum I, Carrère-Kremer S, Blaise M, Viljoen A, Bernut A, Le Moigne V, Vilchèze C,
704 Guérardel Y, Lutfalla G, Herrmann J-L, Jacobs WR, Kremer L.** 2016. Deletion of a
705 dehydratase important for intracellular growth and cording renders rough *Mycobacterium
706 abscessus* avirulent. *Proc. Natl. Acad. Sci. USA* **113**:E4228–37.
- 707 21. **Brambilla C, Llorens-Fons M, Julián E, Noguera-Ortega E, Tomàs-Martínez C, Pérez-
708 Trujillo M, Byrd TF, Alcaide F, Luquin M.** 2016. Mycobacteria clumping increase their
709 capacity to damage macrophages. *Front. Microbiol.* **7**:1562.
- 710 22. **Gebert MJ, Delgado-Baquerizo M, Oliverio AM, Webster TM, Nichols LM, Honda JR,
711 Chan ED, Adjemian J, Dunn RR, Fierer N.** 2018. Ecological analyses of mycobacteria in
712 showerhead biofilms and their relevance to human health. *MBio* **9**.
- 713 23. **Vaerewijck MMJ, Huys G, Palomino JC, Swings J, Portaels F.** 2005. Mycobacteria in
714 drinking water distribution systems: ecology and significance for human health. *FEMS
715 Microbiol. Rev.* **29**:911–934.
- 716 24. **Floto RA, Olivier KN, Saiman L, Daley CL, Herrmann J-L, Nick JA, Noone PG, Bilton
717 D, Corris P, Gibson RL, Hempstead SE, Koetz K, Sabadosa KA, Sermet-Gaudelus I,**

- 718 **Smyth AR, van Ingen J, Wallace RJ, Winthrop KL, Marshall BC, Haworth CS, US Cystic Fibrosis Foundation and European Cystic Fibrosis Society.** 2016. US Cystic Fibrosis Foundation and European Cystic Fibrosis Society consensus recommendations for the management of non-tuberculous mycobacteria in individuals with cystic fibrosis. *Thorax* **71 Suppl 1**:i1–22.
- 723 25. **Field SK, Fisher D, Cowie RL.** 2004. *Mycobacterium avium* complex pulmonary disease in patients without HIV infection. *Chest* **126**:566–581.
- 725 26. **Marras TK, Campitelli MA, Kwong JC, Lu H, Brode SK, Marchand-Austin A, Gershon AS, Jamieson FB.** 2016. Risk of nontuberculous mycobacterial pulmonary disease with obstructive lung disease. *Eur. Respir. J.* **48**:928–931.
- 728 27. **Nessim R, Cambau E, Reyrat JM, Murray A, Gicquel B.** 2012. *Mycobacterium abscessus*: a new antibiotic nightmare. *J. Antimicrob. Chemother.* **67**:810–818.
- 730 28. **Lopeman RC, Harrison J, Desai M, Cox JAG.** 2019. *Mycobacterium abscessus*: Environmental Bacterium Turned Clinical Nightmare. *Microorganisms* **7**.
- 732 29. **Ojha A, Anand M, Bhatt A, Kremer L, Jacobs WR, Hatfull GF.** 2005. GroEL1: a dedicated chaperone involved in mycolic acid biosynthesis during biofilm formation in mycobacteria. *Cell* **123**:861–873.
- 735 30. **Sani M, Houben ENG, Geurtsen J, Pierson J, de Punder K, van Zon M, Wever B, Piersma SR, Jiménez CR, Daffé M, Appelmelk BJ, Bitter W, van der Wel N, Peters PJ.** 2010. Direct visualization by cryo-EM of the mycobacterial capsular layer: a labile structure containing ESX-1-secreted proteins. *PLoS Pathog.* **6**:e1000794.
- 739 31. **Meyers PR, Bourn WR, Steyn LM, van Helden PD, Beyers AD, Brown GD.** 1998. Novel method for rapid measurement of growth of mycobacteria in detergent-free media. *J. Clin. Microbiol.* **36**:2752–2754.
- 742 32. **Julián E, Roldán M, Sánchez-Chardi A, Astola O, Agustí G, Luquin M.** 2010. Microscopic cords, a virulence-related characteristic of *Mycobacterium tuberculosis*, are also present in nonpathogenic mycobacteria. *J. Bacteriol.* **192**:1751–1760.
- 745 33. **Ojha AK, Baughn AD, Sambandan D, Hsu T, Trivelli X, Guerardel Y, Alahari A, Kremer L, Jacobs WR, Hatfull GF.** 2008. Growth of *Mycobacterium tuberculosis* biofilms containing free mycolic acids and harbouring drug-tolerant bacteria. *Mol. Microbiol.* **69**:164–174.
- 749 34. **Ojha A, Hatfull GF.** 2007. The role of iron in *Mycobacterium smegmatis* biofilm formation: the exochelin siderophore is essential in limiting iron conditions for biofilm formation but not for planktonic growth. *Mol. Microbiol.* **66**:468–483.
- 752 35. **Nguyen L, Scherr N, Gatfield J, Walburger A, Pieters J, Thompson CJ.** 2007. Antigen 84, an effector of pleiomorphism in *Mycobacterium smegmatis*. *J. Bacteriol.* **189**:7896–7910.

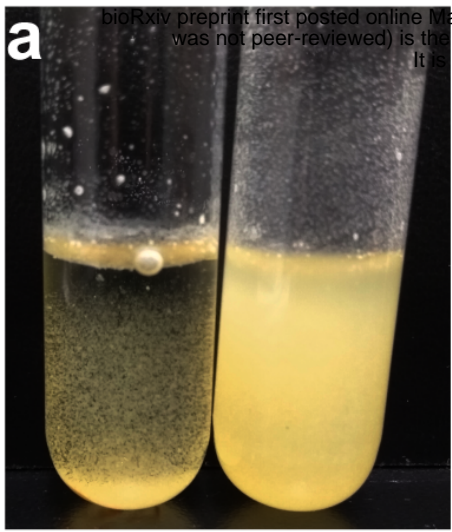
- 755 36. **Monnet V.** 2003. Bacterial oligopeptide-binding proteins. *Cell Mol. Life Sci.* **60**:2100–
756 2114.
- 757 37. **Flores-Valdez MA, Morris RP, Laval F, Daffé M, Schoolnik GK.** 2009. *Mycobacterium*
758 *tuberculosis* modulates its cell surface via an oligopeptide permease (Opp) transport
759 system. *FASEB J.* **23**:4091–4104.
- 760 38. **Vince A, Dawson AM, Park N, O’Grady F.** 1973. Ammonia production by intestinal
761 bacteria. *Gut* **14**:171–177.
- 762 39. **Cook GM, Berney M, Gebhard S, Heinemann M, Cox RA, Danilchanka O, Niederweis**
763 **M.** 2009. Physiology of Mycobacteria, p. 81–319. *In Advances in Microbial Physiology*.
764 Elsevier.
- 765 40. **De Carvalho LPS, Fischer SM, Marrero J, Nathan C, Ehrt S, Rhee KY.** 2010.
766 Metabolomics of *Mycobacterium tuberculosis* reveals compartmentalized co-catabolism of
767 carbon substrates. *Chem. Biol.* **17**:1122–1131.
- 768 41. **Gräzer-Lampart SD, Egli T, Hamer G.** 1986. Growth of *Hyphomicrobium ZV620* in the
769 Chemostat: Regulation of NH₄⁺-assimilating Enzymes and Cellular Composition.
770 *MICROBIOLOGY* **132**:3337–3347.
- 771 42. **Chen N, Huang J, Feng Z, Yu L, Xu Q, Wen T.** 2009. Optimization of fermentation
772 conditions for the biosynthesis of L-threonine by *Escherichia coli*. *Appl. Biochem.*
773 *Biotechnol.* **158**:595–604.
- 774 43. **Aanderud ZT, Saurey S, Ball BA, Wall DH, Barrett JE, Muscarella ME, Griffin NA,**
775 **Virginia RA, Adams BJ.** 2018. Stoichiometric shifts in soil C:N:P promote bacterial taxa
776 dominance, maintain biodiversity, and deconstruct community assemblages. *Front.*
777 *Microbiol.* **9**:1401.
- 778 44. **Johnson MM, Odell JA.** 2014. Nontuberculous mycobacterial pulmonary infections. *J*
779 *Thorac Dis* **6**:210–220.
- 780 45. **Demoling F, Figueroa D, Bååth E.** 2007. Comparison of factors limiting bacterial growth
781 in different soils. *Soil Biol. Biochem.* **39**:2485–2495.
- 782 46. **Aldén L, Demoling F, Bååth E.** 2001. Rapid method of determining factors limiting
783 bacterial growth in soil. *Appl. Environ. Microbiol.* **67**:1830–1838.
- 784 47. **Trevors JT, van Elsas JD, van Overbeek LS, Starodub ME.** 1990. Transport of a
785 genetically engineered *Pseudomonas fluorescens* strain through a soil microcosm. *Appl.*
786 *Environ. Microbiol.* **56**:401–408.
- 787 48. **Parke JL, Moen R, Rovira AD, Bowen GD.** 1986. Soil water flow affects the rhizosphere
788 distribution of a seed-borne biological control agent, *Pseudomonas fluorescens*. *Soil Biol.*
789 *Biochem.* **18**:583–588.

- 790 49. **Gannon JT, Manilal VB, Alexander M.** 1991. Relationship between Cell Surface
791 Properties and Transport of Bacteria through Soil. *Appl. Environ. Microbiol.* **57**:190–193.
- 792 50. **Petridis M, Benjak A, Cook GM.** 2015. Defining the nitrogen regulated transcriptome of
793 *Mycobacterium smegmatis* using continuous culture. *BMC Genomics* **16**:821.
- 794 51. **Berney M, Cook GM.** 2010. Unique flexibility in energy metabolism allows mycobacteria
795 to combat starvation and hypoxia. *PLoS One* **5**:e8614.
- 796 52. **Commichau FM, Forchhammer K, Stüke J.** 2006. Regulatory links between carbon and
797 nitrogen metabolism. *Curr. Opin. Microbiol.* **9**:167–172.
- 798 53. **Litsios A, Ortega ÁD, Wit EC, Heinemann M.** 2018. Metabolic-flux dependent regulation
799 of microbial physiology. *Curr. Opin. Microbiol.* **42**:71–78.
- 800 54. **Kotte O, Zaugg JB, Heinemann M.** 2010. Bacterial adaptation through distributed
801 sensing of metabolic fluxes. *Mol. Syst. Biol.* **6**:355.
- 802 55. **Huergo LF, Dixon R.** 2015. The Emergence of 2-Oxoglutarate as a Master Regulator
803 Metabolite. *Microbiol. Mol. Biol. Rev.* **79**:419–435.
- 804 56. **Marrakchi H, Lanéelle M-A, Daffé M.** 2014. Mycolic acids: structures, biosynthesis, and
805 beyond. *Chem. Biol.* **21**:67–85.
- 806 57. **Vincent AT, Nyongesa S, Morneau I, Reed MB, Tocheva EI, Veyrier FJ.** 2018. The
807 mycobacterial cell envelope: A relict from the past or the result of recent evolution? *Front.
808 Microbiol.* **9**:2341.
- 809 58. **Brennan PJ, Goren MB.** 1979. Structural studies on the type-specific antigens and lipids
810 of the *Mycobacterium avium*. *Mycobacterium intracellulare*. *Mycobacterium scrofulaceum*
811 serocomplex. *Mycobacterium intracellulare* serotype 9. *J. Biol. Chem.* **254**:4205–4211.
- 812 59. **Chiaradia L, Lefebvre C, Parra J, Marcoux J, Burlet-Schiltz O, Etienne G, Tropis M,
813 Daffé M.** 2017. Dissecting the mycobacterial cell envelope and defining the composition of
814 the native mycomembrane. *Sci. Rep.* **7**:12807.
- 815 60. **Koch R.** 1932. Die aetiologie der tuberkulose, a translation by Berna Pinner and Max
816 Pinner with an introduction by Allen K. Krause. *Am Rev Tuberc* 285–323.
- 817 61. **Middlebrook G, Dubos RJ, Pierce C.** 1947. Virulence and morphological characteristics
818 of mammalian tubercle bacilli. *J. Exp. Med.* **86**:175–184.
- 819 62. **Pierce C, Dubos RJ, Middlebrook G.** 1947. Infection of mice with mammalian tubercle
820 bacilli grown in tween-albumin liquid medium. *J. Exp. Med.* **86**:159–174.
- 821 63. **S. Glickman M.** 2008. 5 cording, cord factors, and trehalose dimycolate, p. 63–73. *In*
822 Avenir, G, Daffé, M, Reyrat, J-M (eds.), *The mycobacterial cell envelope*. American
823 Society of Microbiology.

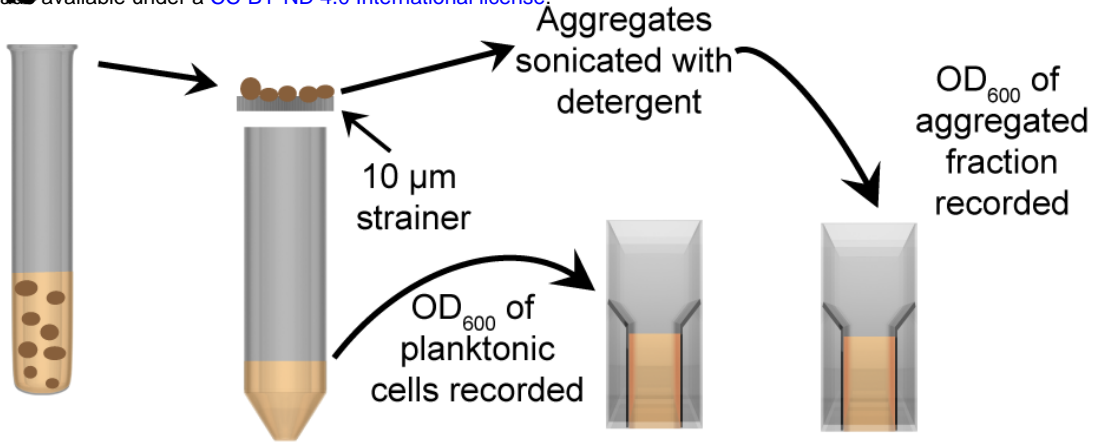
- 824 64. **Bloch H.** 1950. Studies on the virulence of tubercle bacilli; isolation and biological
825 properties of a constituent of virulent organisms. *J. Exp. Med.* **91**:197–218, pl.
- 826 65. **Noll H, Bloch H, Asselineau J, Lederer E.** 1956. The chemical structure of the cord
827 factor of *Mycobacterium tuberculosis*. *Biochim. Biophys. Acta* **20**:299–309.
- 828 66. **Matsunaga I, Naka T, Talekar RS, McConnell MJ, Katoh K, Nakao H, Otsuka A, Behar
829 SM, Yano I, Moody DB, Sugita M.** 2008. Mycolyltransferase-mediated glycolipid
830 exchange in Mycobacteria. *J. Biol. Chem.* **283**:28835–28841.
- 831 67. **Bhatt A, Fujiwara N, Bhatt K, Gurcha SS, Kremer L, Chen B, Chan J, Porcelli SA,
832 Kobayashi K, Besra GS, Jacobs WR.** 2007. Deletion of kasB in *Mycobacterium
833 tuberculosis* causes loss of acid-fastness and subclinical latent tuberculosis in
834 immunocompetent mice. *Proc. Natl. Acad. Sci. USA* **104**:5157–5162.
- 835 68. **Baba T, Kaneda K, Kusunose E, Kusunose M, Yano I.** 1989. Thermally adaptive
836 changes of mycolic acids in *Mycobacterium smegmatis*. *J. Biochem.* **106**:81–86.
- 837 69. **Etienne G, Villeneuve C, Billman-Jacobe H, Astarie-Dequeker C, Dupont M-A, Daffé
838 M.** 2002. The impact of the absence of glycopeptidolipids on the ultrastructure, cell
839 surface and cell wall properties, and phagocytosis of *Mycobacterium smegmatis*.
840 *Microbiology (Reading, Engl)* **148**:3089–3100.
- 841 70. **Ojha AK, Varma S, Chatterji D.** 2002. Synthesis of an unusual polar glycopeptidolipid in
842 glucose-limited culture of *Mycobacterium smegmatis*. *Microbiology (Reading, Engl)*
843 **148**:3039–3048.
- 844 71. **Yamazaki Y, Danelishvili L, Wu M, Macnab M, Bermudez LE.** 2006. *Mycobacterium
845 avium* genes associated with the ability to form a biofilm. *Appl. Environ. Microbiol.* **72**:819–
846 825.
- 847 72. **Howard ST, Rhoades E, Recht J, Pang X, Alsup A, Kolter R, Lyons CR, Byrd TF.**
848 2006. Spontaneous reversion of *Mycobacterium abscessus* from a smooth to a rough
849 morphotype is associated with reduced expression of glycopeptidolipid and reacquisition
850 of an invasive phenotype. *Microbiology (Reading, Engl)* **152**:1581–1590.
- 851 73. **Mukherjee R, Gomez M, Jayaraman N, Smith I, Chatterji D.** 2005. Hyperglycosylation
852 of glycopeptidolipid of *Mycobacterium smegmatis* under nutrient starvation: structural
853 studies. *Microbiology (Reading, Engl)* **151**:2385–2392.
- 854 74. **Kim B-J, Kim B-R, Lee S-Y, Kook Y-H, Kim B-J.** 2013. Rough colony morphology of
855 *Mycobacterium massiliense* Type II genotype is due to the deletion of glycopeptidolipid
856 locus within its genome. *BMC Genomics* **14**:890.
- 857 75. **Pawlak A, Garnier G, Orgeur M, Tong P, Lohan A, Le Chevalier F, Sapriel G, Roux A-
858 L, Conlon K, Honoré N, Dillies M-A, Ma L, Bouchier C, Coppée J-Y, Gaillard J-L,
859 Gordon SV, Loftus B, Brosch R, Herrmann JL.** 2013. Identification and characterization

- 860 of the genetic changes responsible for the characteristic smooth-to-rough morphotype
861 alterations of clinically persistent *Mycobacterium abscessus*. Mol. Microbiol. **90**:612–629.
- 862 76. **Van Kessel JC, Marinelli LJ, Hatfull GF.** 2008. Recombineering mycobacteria and their
863 phages. Nat. Rev. Micro. **6**:851–857.
- 864 77. **Costa KC, Bergkessel M, Saunders S, Korlach J, Newman DK.** 2015. Enzymatic
865 Degradation of Phenazines Can Generate Energy and Protect Sensitive Organisms from
866 Toxicity. MBio **6**:e01520–15.
- 867 78. **Bolger AM, Lohse M, Usadel B.** 2014. Trimmomatic: a flexible trimmer for Illumina
868 sequence data. Bioinformatics **30**:2114–2120.
- 869 79. **Li H, Durbin R.** 2009. Fast and accurate short read alignment with Burrows-Wheeler
870 transform. Bioinformatics **25**:1754–1760.
- 871 80. **Li H, Handsaker B, Wysoker A, Fennell T, Ruan J, Homer N, Marth G, Abecasis G,**
872 **Durbin R, 1000 Genome Project Data Processing Subgroup.** 2009. The Sequence
873 Alignment/Map format and SAMtools. Bioinformatics **25**:2078–2079.
- 874 81. **DePristo MA, Banks E, Poplin R, Garimella KV, Maguire JR, Hartl C, Philippakis AA,**
875 **del Angel G, Rivas MA, Hanna M, McKenna A, Fennell TJ, Kernytsky AM,**
876 **Sivachenko AY, Cibulskis K, Gabriel SB, Altshuler D, Daly MJ.** 2011. A framework for
877 variation discovery and genotyping using next-generation DNA sequencing data. Nat.
878 Genet. **43**:491–498.
- 879 82. **Cingolani P, Platts A, Wang LL, Coon M, Nguyen T, Wang L, Land SJ, Lu X, Ruden**
880 **DM.** 2012. A program for annotating and predicting the effects of single nucleotide
881 polymorphisms, SnpEff: SNPs in the genome of *Drosophila melanogaster* strain w1118;
882 iso-2; iso-3. Fly (Austin). **6**:80–92.
- 883

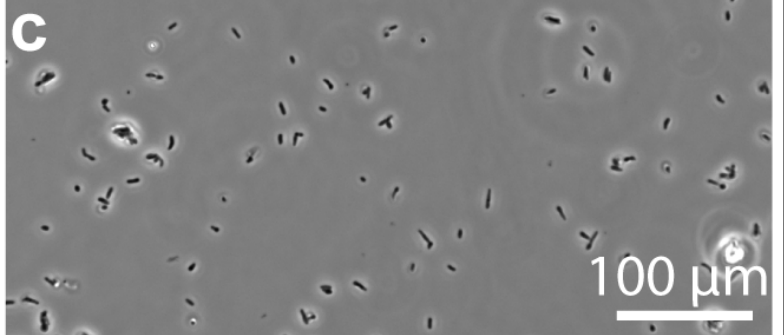
a



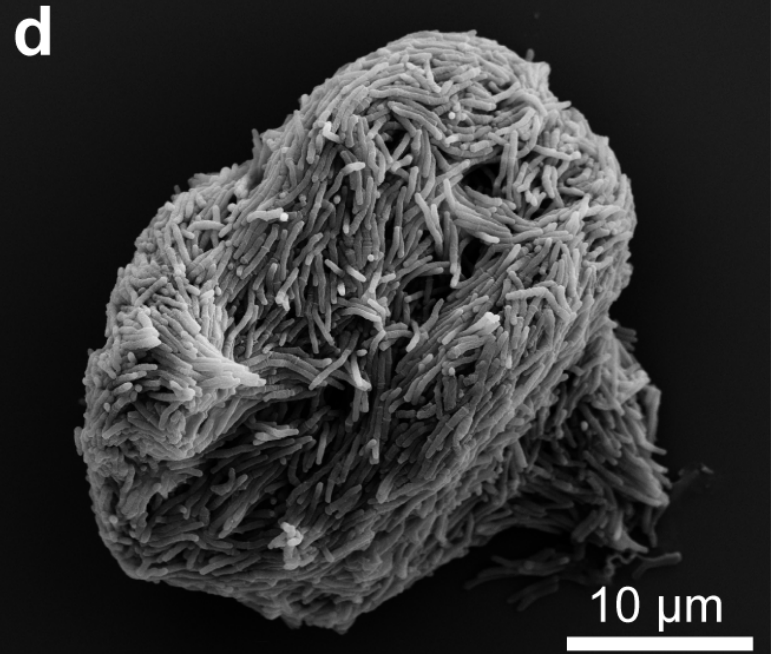
b



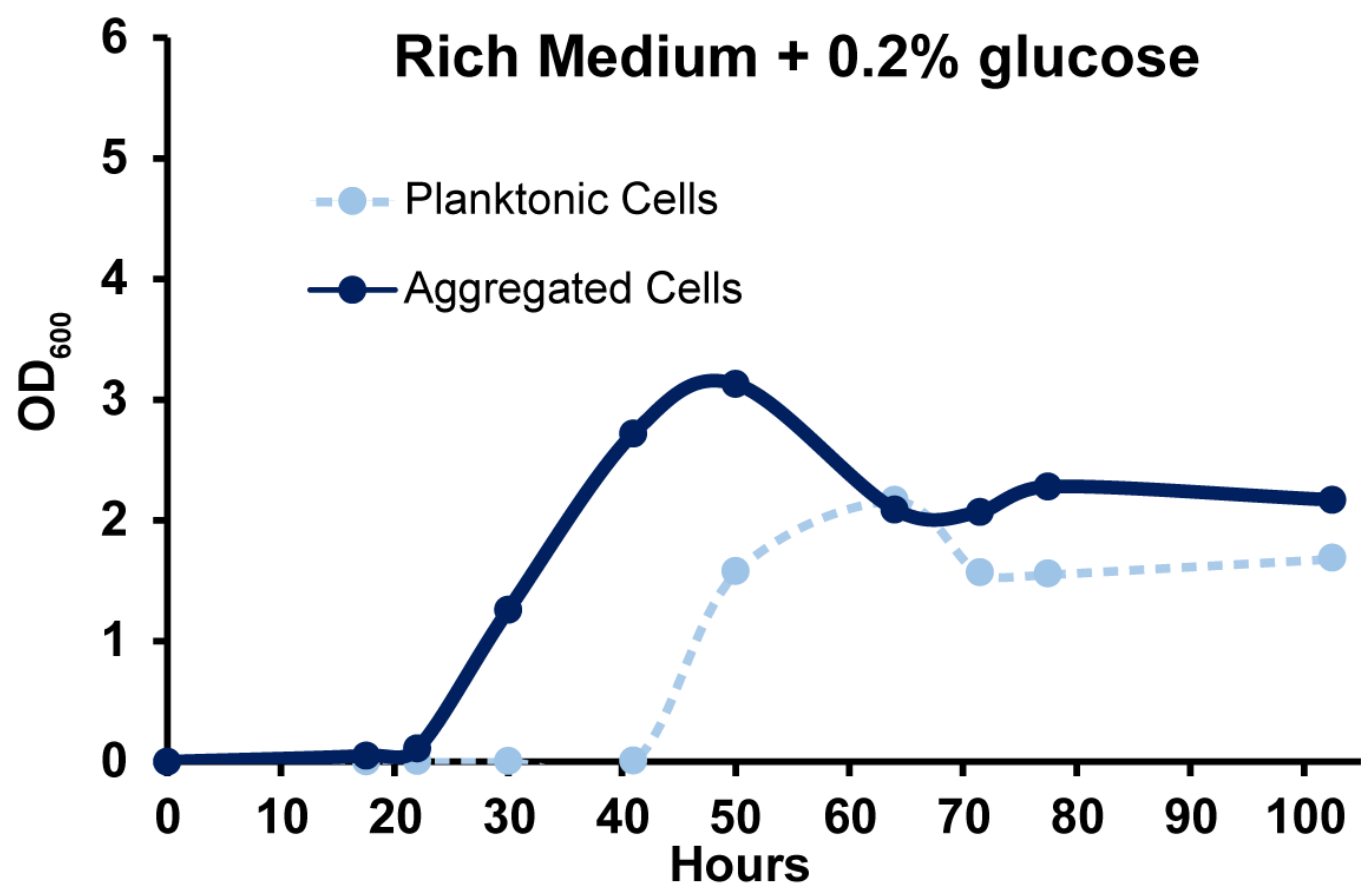
c



d



e



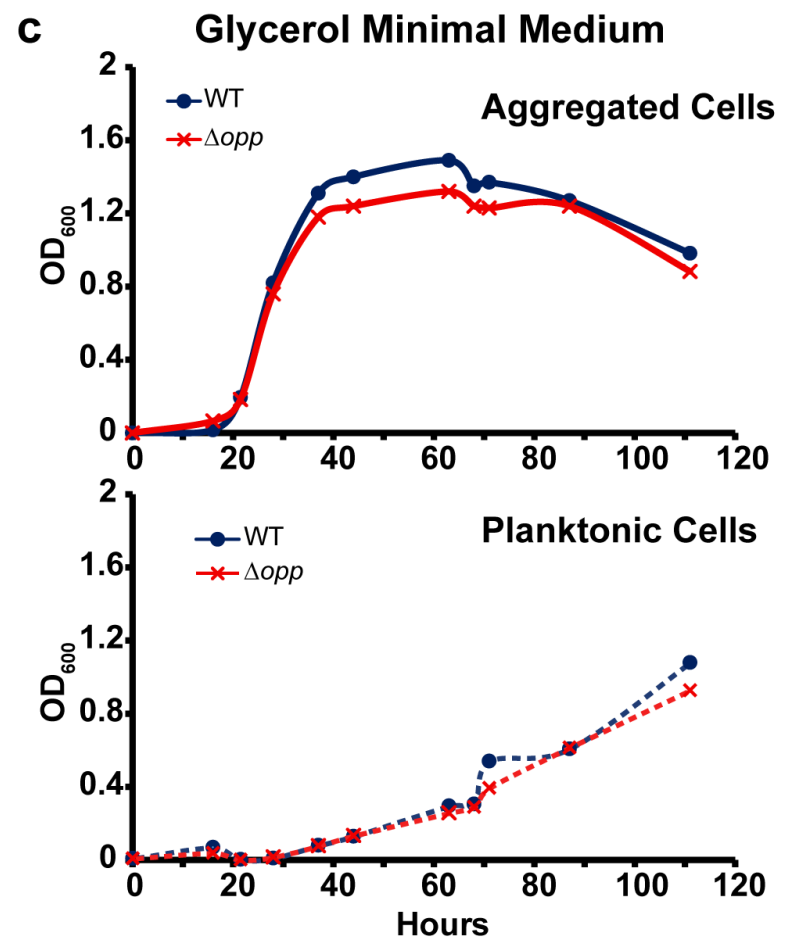
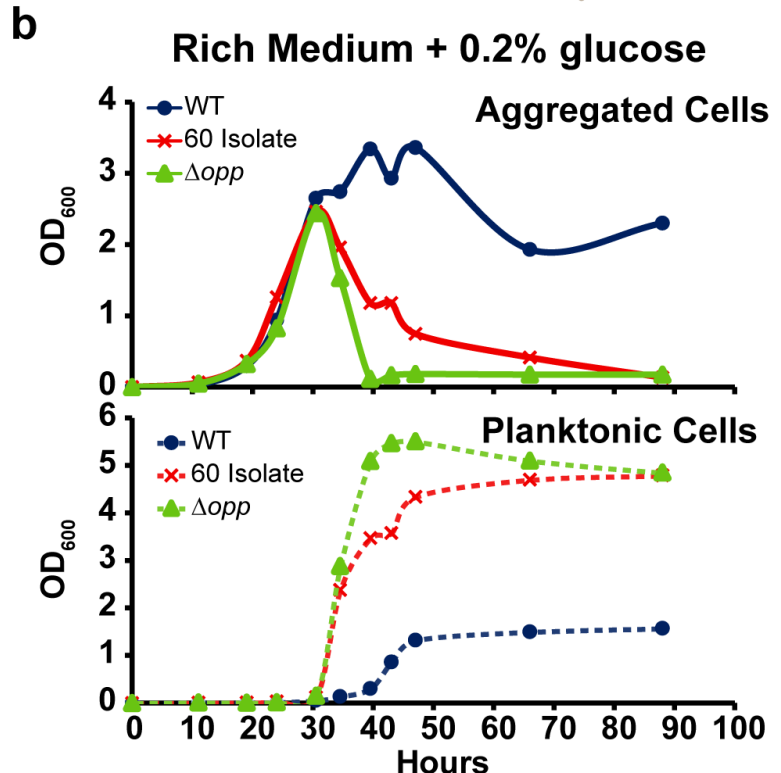
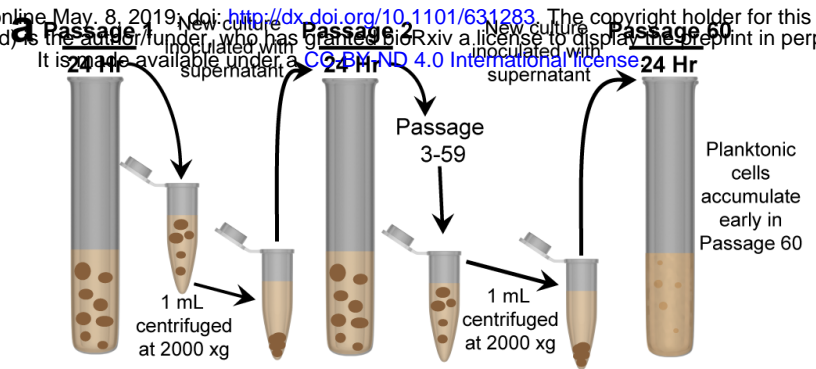


Table 1

	Gene	Function	Mutation Type	Mutation
Pass 40	MSMEG_1808	SufE	Missense	Glu39Val
	MSMEG_2148	HNH endonuclease domain-containing protein	Frameshift	Ser534fs *
	MSMEG_5061	Extracellular solute binding protein	Missense	Ser249Pro
	MSMEG_5808	Binding protein dependent transporter	Missense	Arg117Cys
	MSMEG_6397	Hypothetical protein	Missense	Ser21Pro
	MSMEG_6430	Hypothetical protein	Missense	Thr371Lys
	MSMEG_6821	NLP/P60 family protein	Missense	Gln2017Arg

	Gene	Function	Mutation Type	Mutation
Pass 60	MSMEG_0639	Oligopeptide transport ATP-binding protein OppF	Frameshift	Lys12fs #
	MSMEG_0640	Oligopeptide transport ATP-binding protein OppD	Missense	Phe96Leu
	MSMEG_2148	HNH endonuclease domain-containing protein	Missense	Pro380Arg
	MSMEG_2148	HNH endonuclease domain-containing protein	Frameshift	Ser534fs *
	MSMEG_3677	Serine/Threonine protein kinase	Silent	Val320Val
	MSMEG_4217	DivIVA protein	Missense	Glu107Gly
	MSMEG_5061	Extracellular solute binding protein	Frameshift	Glu225fs &
	MSMEG_5395	Sensor Histidine Kinase KdpD	Missense	Arg627Cys
	MSMEG_6497	Hypothetical protein	Missense	His43Gln

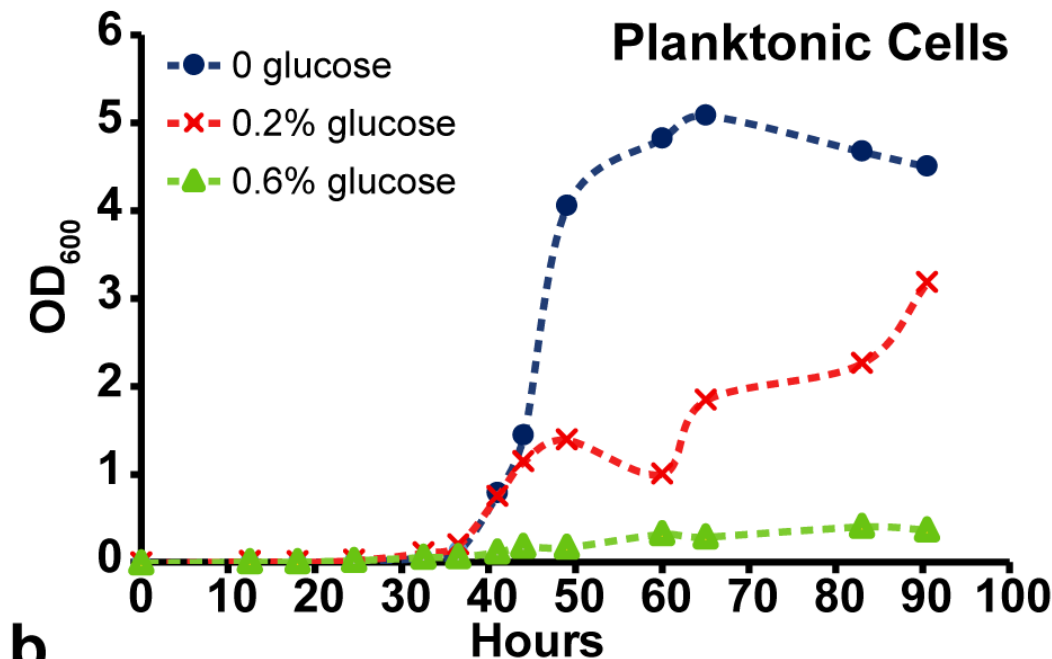
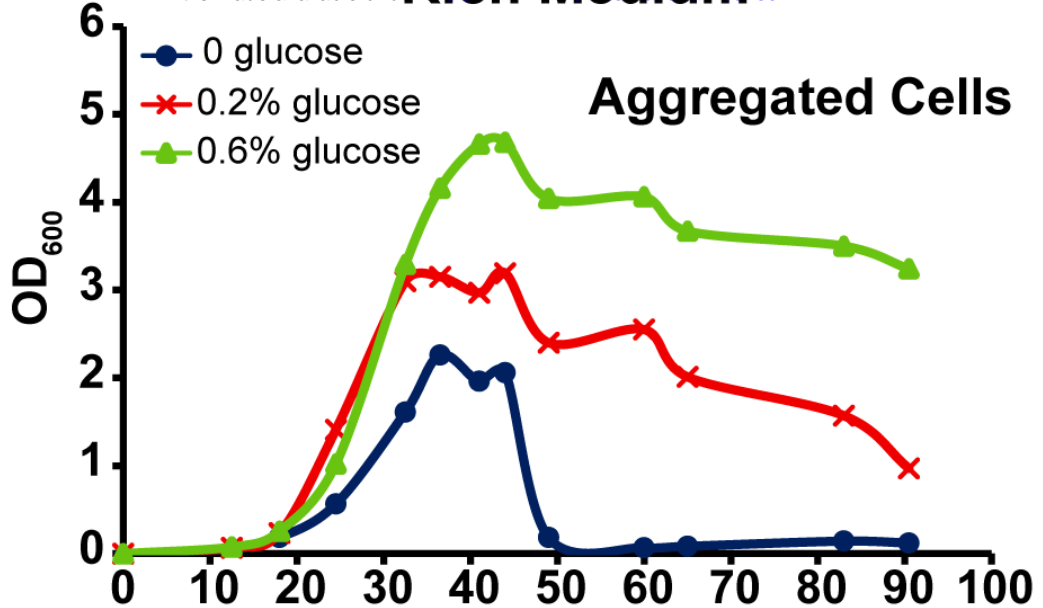
Red text indicates the genes that were mutated in WT to test for aggregation defects

* - MSMEG_2148 is 544 amino acids. Ser534 frameshift hypothetically replaces the 8 C-terminal amino acids with a different 23 amino acid sequence.

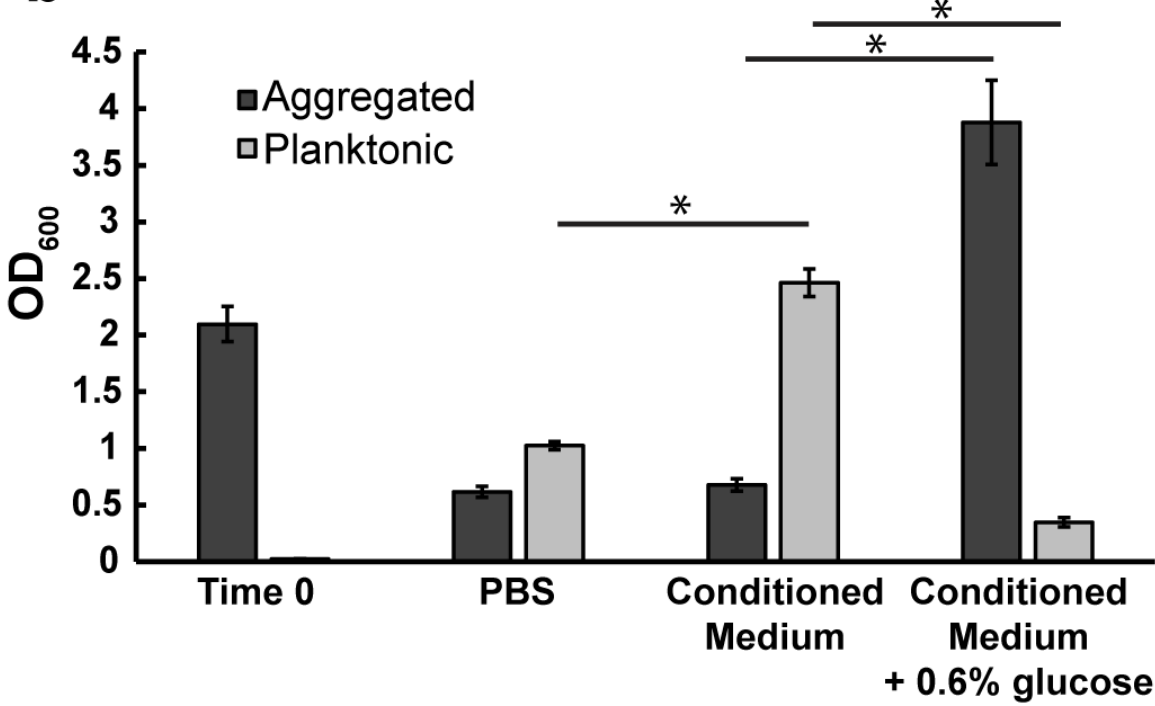
- MSMEG_0639 is 336 amino acids. Lys12 frameshift hypothetically replaces the 325 C-terminal amino acids with a different 24 amino acid sequence.

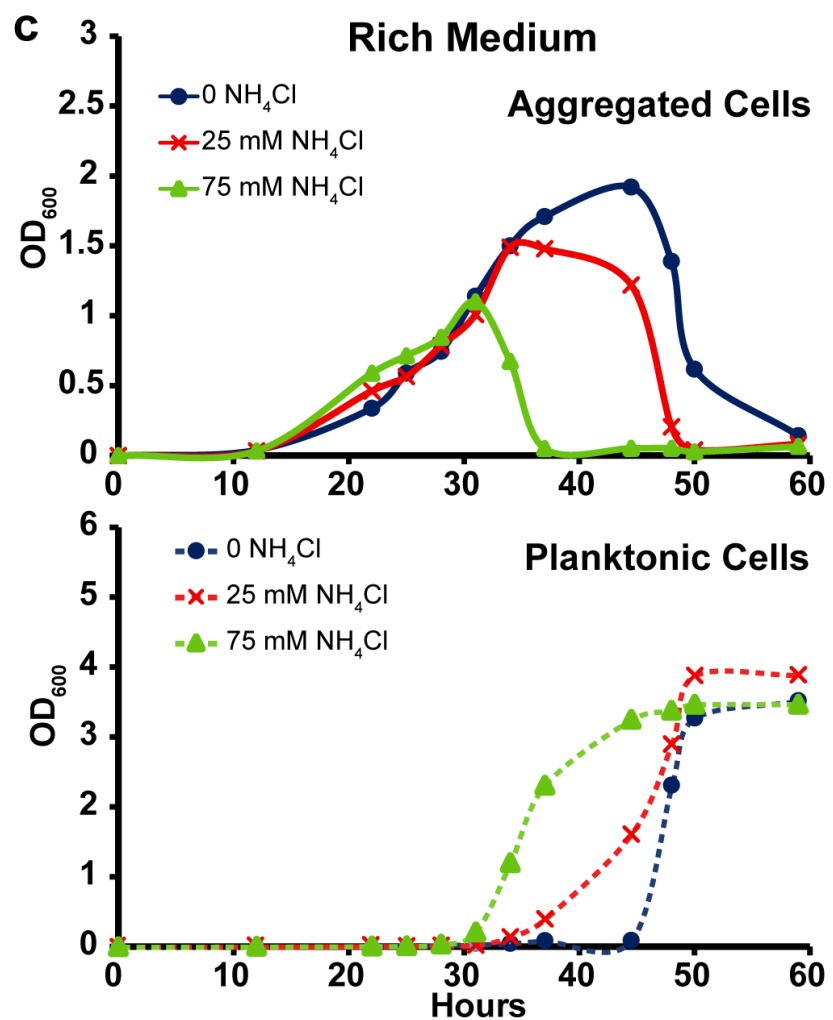
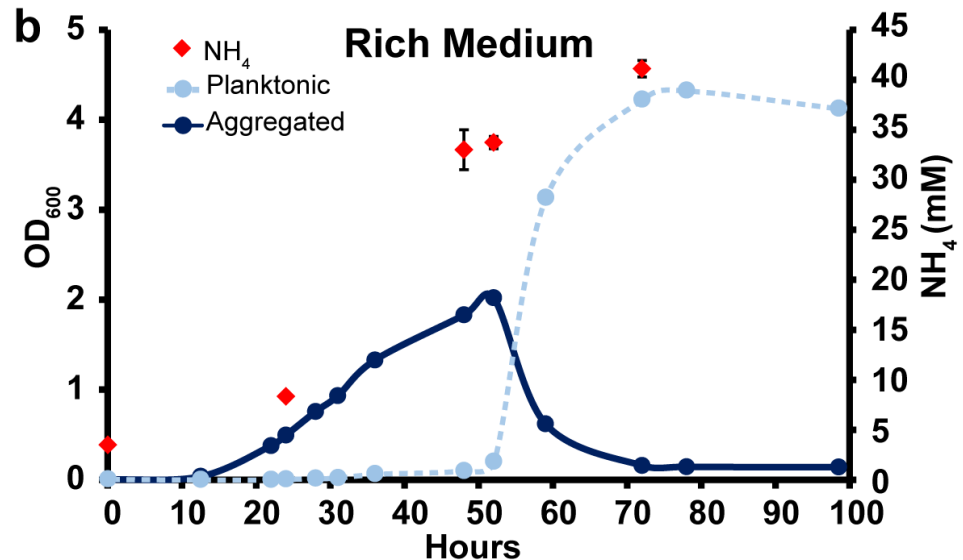
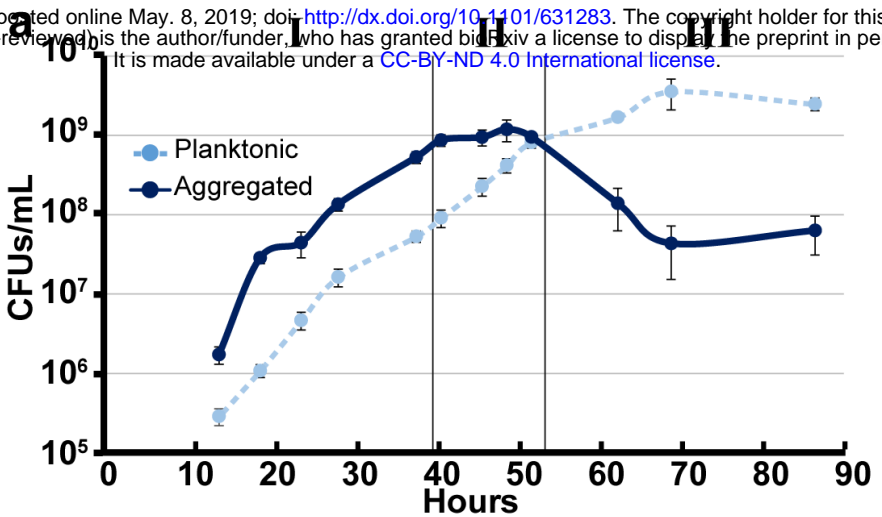
& - MSMEG_5061 is 465 amino acids. Glu225 frameshift hypothetically replaces the 241 C-terminal acids with a different 236 amino acid sequence.

a Rich Medium

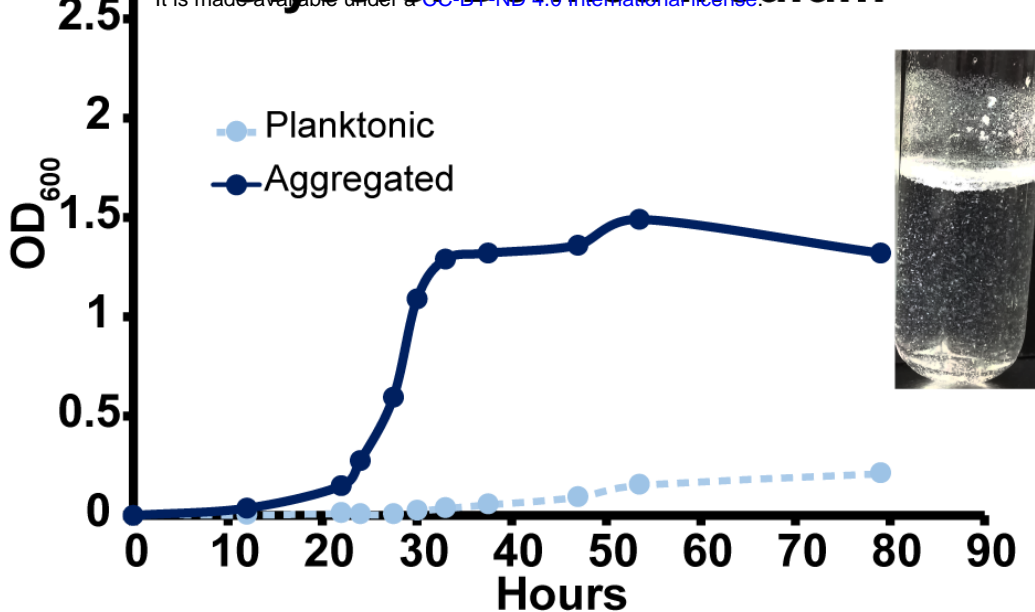


b

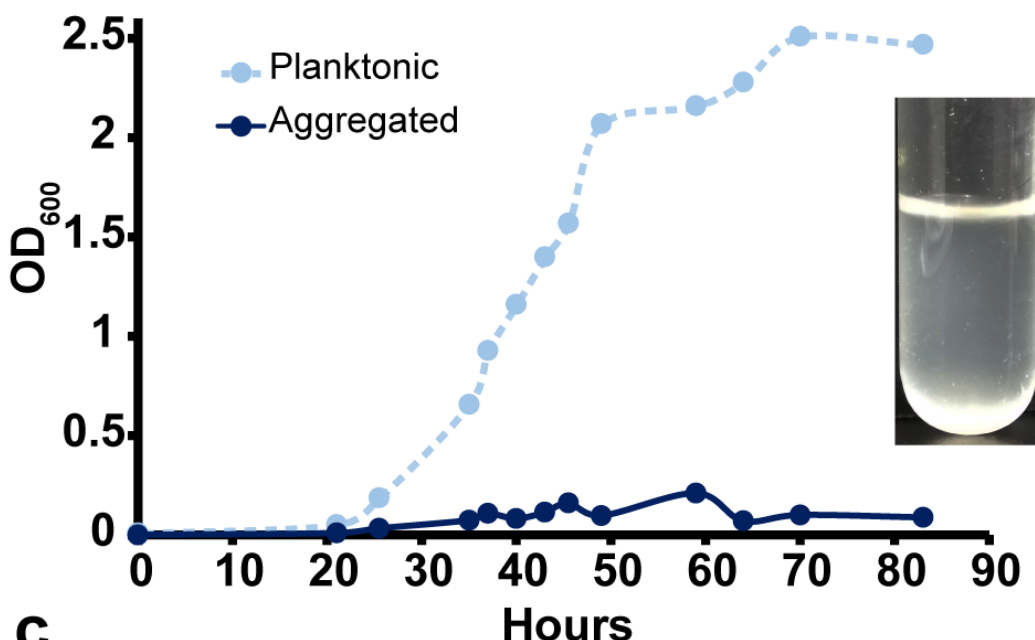




a Glycerol Defined Medium



b Pyruvate Defined Medium



c

